Green Chemistry

PAPER

View Article Online
View Journal | View Issue

Cite this: *Green Chem.*, 2026, **28**, 2622

Cyclodesulfurization reaction catalyzed by artificial metalloenzymes containing cobalt protoporphyrin IX cofactors under green aqueous solvent conditions

Xinjia Yu,†[a] Yutong Li,†[a] Fengxi Li,[a] Shenhan Xie,[a] Liang Li,[c] Hong Zhang,*[b] Zhi Wang*[a] and Lei Wang*[a]

Received 26th November 2025,
Accepted 9th January 2026

DOI: 10.1039/d5gc06364g

rsc.li/greenchem

In this study, we report the development of an environmentally friendly artificial *Vitreoscilla* hemoglobin (VHb) for the synthesis of 3-amino-[1,2,4]-triazole and [4,3-*a*]pyridine. We employed a strategy that combines porphyrin substitution with axial ligand mutations to create a highly active VHb oxidase containing cobalt protoporphyrin IX (Co(ppIX)), while simultaneously introducing double mutations (H85Y, P54C). This artificial enzyme catalyzes the cyclization desulfurization reaction of the corresponding 2-hydrazinopyridine and isothiocyanate in PBS containing 10% DMSO (v/v) under aerobic conditions at room temperature. This method addresses the limitations of catalytic activity observed in natural hemoglobin and provides a novel pathway for the green synthesis of nitrogen-containing heterocycles. Furthermore, the porphyrin ligand substitution strategy broadens the application scope of artificial metalloenzymes in non-natural reactions.

Green foundation

1. A rationally engineered artificial metalloenzyme (VHb-Co(H85Y, P54C)) enables biocatalytic green synthesis of pharmaceutical 3-amino-[1,2,4]-triazolo[4,3-*a*]pyridines *via* aqueous cyclodesulfurization, overcoming traditional route drawbacks through biocatalysis's mild, specific, low-toxicity and optimized hemoglobin active site cofactors.
2. Engineered VHb-Co (H85Y, P54C) delivers a high yield for target model heterocycle substrates with a low loading of catalyst and an aqueous solvent system. The room-temperature, O2-driven process eschews toxic reagents and metals, and harnesses biocatalysis' merits alongside optimized hemoglobin active sites and cofactors to overcome traditional synthesis flaws.
3. Subsequent studies could explore cascade reactions using the same artificial metalloenzyme to synthesize target heterocycles directly from simple, renewable precursors eliminating intermediate isolation steps

Introduction

The 1,2,4-triazolo[4,3-*a*]pyridine scaffold is a highly significant heterocyclic unit in organic synthesis, frequently encountered in functional molecules with notable biological activities.[1] Research has demonstrated that compounds containing this core structure exhibit a wide range of pharmacological activities (Fig. 1a), including antibacterial, anti-inflammatory, antitumor, antiepileptic, and anticonvulsant effects.[2] Due to their considerable potential in drug development, the efficient synthesis and methodological innovation of this scaffold have long been focal points of research in organic chemistry.[3] Despite significant advancements in these synthetic studies, existing methodologies still suffer from limitations, such as high catalyst loading, harsh reaction conditions, and reliance on strong oxidants or toxic reagents. To address these issues, our group recently developed a novel visible-light-driven catalytic green synthesis strategy, which has further enriched the library of synthetic methods for this heterocyclic scaffold[4] (Fig. 1b). However, the green synthetic strategies for this heterocyclic scaffold still require further expansion.[5] Consequently, the development of more environmentally benign and mild protocols for constructing the 1,2,4-triazolo[4,3-*a*]pyridine scaffold remains of considerable practical significance.

[a]*Key Laboratory of Molecular Enzymology and Engineering of Ministry of Education, School of Life Sciences, Jilin University, Changchun 130023, P. R. China. E-mail: wangzhi@jlu.edu.cn, w_lei@jlu.edu.cn*
[b]*Institute for Interdisciplinary Biomass Functional Materials Studies, Jilin Engineering Normal University, Kaixuan Road 3050, Changchun, 130052, P. R. China. E-mail: zhanghong0825@jlenu.edu.cn*
[c]*Department of Industry and Information Technology of Jilin Province, 199 Jianshe Street, Kuancheng District, Changchun 130000, P. R. China. E-mail: 15810006169@163.com*
†These authors contributed equally to this work.

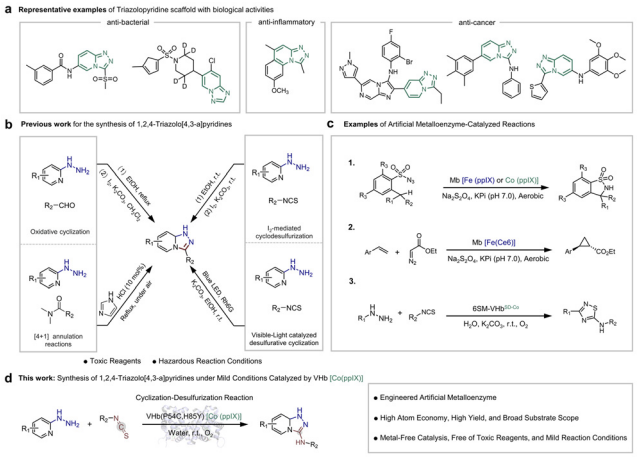

Fig. 1 Mild-condition synthesis of bioactive 1,2,4-triazolo[4,3-*a*]pyridines *via* engineered artificial metalloenzymes. (a) Representative examples of 1,2,4-triazolo[4,3-*a*]pyridine scaffolds with biological activities. (b) Previous work for the synthesis of 1,2,4-triazolo[4,3-*a*]pyridines. (c) Examples of artificial metalloenzyme-catalyzed reactions. (d) This work: the cyclization – desulfurization reaction is catalyzed by VHb [Co(ppIX)].

Biocatalysis, characterized by its environmental friendliness, high efficiency, and specificity, is fundamentally revolutionizing the paradigms of traditional organic synthesis and emerging as an increasingly favored synthetic strategy in organic chemistry.[6] Among these, enzymes as green biocatalysts exhibit exceptional catalytic performance, enabling a series of non-natural transformations under mild conditions and overcoming the dependencies of conventional chemical synthesis on metal catalysts, toxic reagents, and harsh reaction conditions.[7] Notably, hemoglobins, a class of multifunctional biomacromolecules containing heme cofactors, have recently emerged as a research hotspot in the field of green biocatalysis due to their unique catalytic potential. They efficiently mediate various reaction types, such as epoxidation, hydroxylation, and carbene transfer, through their iron-porphyrin active sites while leveraging their distinctive protein cavities to precisely control the stereoselectivity and regioselectivity of reactions.[8] However, the catalytic activity of natural hemoglobin is constrained by the inherent reactivity of its heme iron center. Through directed substitution with artificial metal cofactors, one can precisely regulate the redox potential, ligand field effect, and steric hindrance of the metal center, thereby endowing the protein with novel catalytic functions.[9]

For instance, in 2014, Fasan's group replaced the heme cofactor of myoglobin (Mb) with Mn(ppIX) or Co(ppIX) to enable efficient catalysis of intramolecular C(sp^3)–H amination of aryl sulfonyl azides (Fig. 1c-1). In 2017, they further confirmed that engineered Mb conjugated with chlorin iron e6 could catalyze stereoselective cyclopropanation of olefins (Fig. 1c-2).[10] In light of recent advancements in hemoglobin protein engineering, our team has conducted related research. We replaced the cofactor of *Vitreoscilla* hemoglobin with various metal porphyrins and, utilizing directed evolution techniques, developed a novel artificial metal oxidase. These artificial metal enzymes were employed to efficiently synthesize a range of nitrogen-containing heterocycles, including 2-amino benzo[*d*]oxazole/thiazole and thiazole.[11] Building on our group's prior research findings, VHb and its artificial metal enzymes have exhibited significant potential in catalyzing novel non-natural reactions. Consequently, in this study, we further explored the application of VHb artificial metal oxidase in the cyclization desulfurization reaction, successfully achieving the efficient synthesis of 3-amino-[1,2,4]-triazolo[4,3-*a*]pyridine (Fig. 1d). Notably, this reaction was performed at room temperature using PBS as the reaction medium and O_2 as the oxidant. Compared to previously reported methods, our approach presents substantial advantages in terms of low toxicity and high process safety, while minimizing the reliance on organic solvents.

Results and discussion

First, we selected 2-hydrazinopyridine (**1a**) and phenyl isothiocyanate (**2a**) as model substrates, and evaluated the feasibility of the proposed method through a series of experiments (Fig. 2a). The reaction was performed in a system using PBS (10% DMSO, v/v) as the solvent under an oxygen atmosphere. The results showed that the reaction could not proceed spontaneously without a catalyst (entry 1). Subsequently, we investigated the catalytic activity of wild-type VHb (with hemin as a cofactor) as a biocatalyst (entry 2), which afforded only 16% yield of the target product. Referring to the previously reported metal porphyrin replacement strategy, we substituted the natural hemin in VHb with Co(ppIX), Zn(ppIX), and Mn(ppIX), respectively.[12] We then expressed VHb containing Co(ppIX) in *Escherichia coli* Nissle 1917, achieving a satisfactory yield (14 mg protein per liter of culture) (Fig. 2b). We also sys-

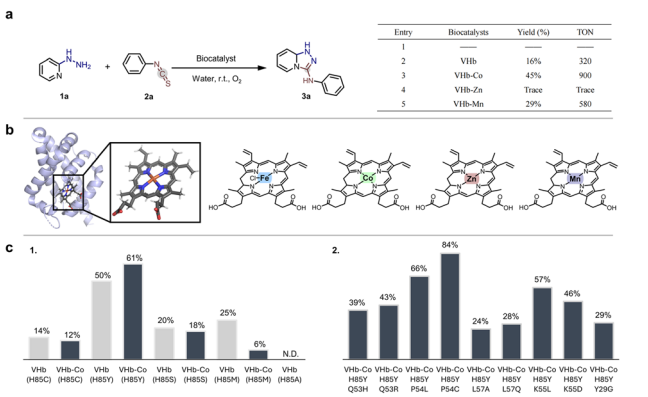

Fig. 2 Screening for the optimal biocatalyst for the synthesis of **3a**. Reaction condition: 2-hydrazinopyridine (**1**, 0.05 mmol), isothiocyanate (**2**, 0.05 mmol), VHb-Co (H85Y, P54C) (Co(ppIX)) (containing 0.05 mol%), PBS (50 mM, 10% DMSO v/v), rt, O_2, 12 h. (a) Screening of the optimal biocatalyst. (b) Replacement of different metalloporphyrins. (c) Screening of VHb mutants.

tematically evaluated the catalytic efficiency of these engineered VHb variants as biocatalysts in this reaction (entries 3–5). The results demonstrated that when VHb-Co alone was used as the catalyst, the reaction yield was significantly higher than that with wild-type VHb-Co. Therefore, VHb-Co was identified as the optimal biocatalyst for further studies (detailed data on the optimization of reaction conditions, including solvents, enzyme dosage, reaction time, pH, and VHb containing different metalloporphyrins, are provided in Table S1 of the SI).

To further enhance catalytic activity, we focused on engineering modifications of the active site of VHb. By integrating data from previous studies on VHb mutants, we constructed an artificial mutant enzyme library. These mutations may alter the coordination environment with metal porphyrin cofactors and the binding modes with reactants by changing the amino acid residues at the active site of VHb. Among these residues, the proximally conserved histidine (H85) is crucial for VHb function, as it not only directly coordinates axially with the metal ligands but also fine-tunes the electronic density on the metal through the electronic effects of its side chain, thereby further influencing the redox properties of VHb.[13] Consequently, axial ligands represent a key factor that dictates the catalytic potential of the active site. Based on this structural analysis, we first selected VHb variants with mutations at the H85 residue to recombine with Co(ppIX) and evaluated the catalytic efficiency of the mutants and recombinant proteins against substrates **1a** and **2a**, respectively (Fig. 2c-1).

The results indicated that the vast majority of H85 mutants were unable to establish effective axial coordination with Co(ppIX), resulting in catalytic product yields ranging from 6% to 25%. Notably, the catalytic product yields of these H85 mutant enzymes were comparable to those of the wild-type VHb. In contrast, the VHb (H85Y) variant exhibited significantly enhanced catalytic performance, with a yield of 50%, and an even higher yield of 61% when bound to Co(ppIX). This substantial difference can be attributed to the fact that the phenolic hydroxyl side chain of tyrosine forms more stable axial coordination bonds with the cobalt at the center of Co(ppIX) through its oxygen atoms, compared to histidine. Additionally, the moderate electron-donating ability of tyrosine adjusts the electron density at the center of Co(ppIX) to an optimal level for substrate activation and electron transfer. Consequently, we performed further screening based on the H85Y variant (Fig. 2c-2). The results revealed that, except for the double mutants VHb-Co (H85Y, P54L) and VHb-Co (H85Y, P54C), the catalytic performance of all other double mutants was inferior to that of the single mutant VHb (H85Y). These findings suggest that mutations at non-axial sites can only fine-tune the microenvironment of the active cavity and cannot substitute for the essential role of functional axial ligands. Notably, the VHb-Co (H85Y, P54C) variant achieved a catalytic product yield of 84% and a turnover number (TON) of 1680 (Table S2, entry 13), demonstrating substantially enhanced catalytic performance that significantly outperforms all other engineered variants. Sulfate-polyacrylamide gel electrophoresis (SDS-PAGE) exhibited a single, distinct band at the expected molecular weight (17 kDa), which matched the theoretical molecular weight of the VHb variant. The electrophoretic patterns obtained confirmed the high homogeneity of the protein preparations. Collectively, these results confirm that the mutant enzyme achieved proper folding and maintained structural integrity throughout expression and purification, thereby providing a critical structural foundation for its superior catalytic performance. Detailed data for screening VHb mutants, including comprehensive catalytic performance data for both single and double mutants within the constructed enzyme library, are provided in Table S2 of the SI.

To further understand the reaction pathway and provide a theoretical basis for exploring substrate applicability, we conducted systematic mechanistic investigations of the cyclic desulfurization reaction catalyzed by VHb-Co (H85Y, P54C). Subsequently, a series of control experiments were performed, and the results are presented in Fig. 3a. First, a radical trapping experiment was conducted in which three equivalents of the radical scavenger TEMPO were added to the reaction system while keeping other parameters unchanged (Fig. 3a-1). The results indicated that only a trace amount of the target product **3a** was detected, even after continuous stirring for 12 hours under standard conditions. This finding suggests that the reaction may involve radical intermediates. When nitrogen (N_2) was used to replace oxygen (O_2) in the system, no target product **3a** was detected (Fig. 3a-2), indicating that O_2 is essential for maintaining the catalytic activity of VHb-Co (H85Y, P54C). Furthermore, under catalyst-free and oxygen-free conditions, intermediate **I** was obtained with a yield of 72% (Fig. 3a-3); however, after adding VHb-Co (H85Y, P54C) and bubbling air, intermediate **I** was ultimately converted to **3a** with a yield of 86% (Fig. 3a-4). In summary, intermediate **II** is a key intermediate in this reaction pathway. Subsequently, utilizing the property of hydrogen peroxide (H_2O_2) to rapidly oxidize ferrous iron (Fe^{2+}) to ferric iron (Fe^{3+}), Mohr's salt solution was added to detect the generation of hydrogen peroxide during the reaction[14] (Fig. 3b). Under standard reaction conditions, with a total reaction duration of 12 hours, the reaction system was centrifuged after 8 hours. Following centrifugation, Mohr's salt solution was added to the supernatant, and the rapid formation of ferric hydroxide flocs was immediately observed. After further centrifugation, distinct precipitates were noted. This result indicates that H_2O_2 is produced during this reaction process.

To further investigate substrate binding to proteins and analyze the stability and interactions of substrate-protein complexes, we docked intermediate **II** into the active cavities of WT-VHb-Co and VHb-Co (H85Y, P54C) respectively using the AutoDock Vina tool within Chimera (the structure of VHb-Co (H85Y, P54C) was constructed by homology modeling strategy using SWISS-MODEL).[15] Fig. 3d illustrates the interactions between intermediate **II** and both WT-VHb-Co and VHb-Co (H85Y, P54C). As shown in Fig. 3d-1, within the active pocket of WT-VHb-Co, intermediate **II** is only embedded in the marginal region of the hydrophobic cavity, exhibiting limited interactions with surrounding residues. Additionally, the sulfur

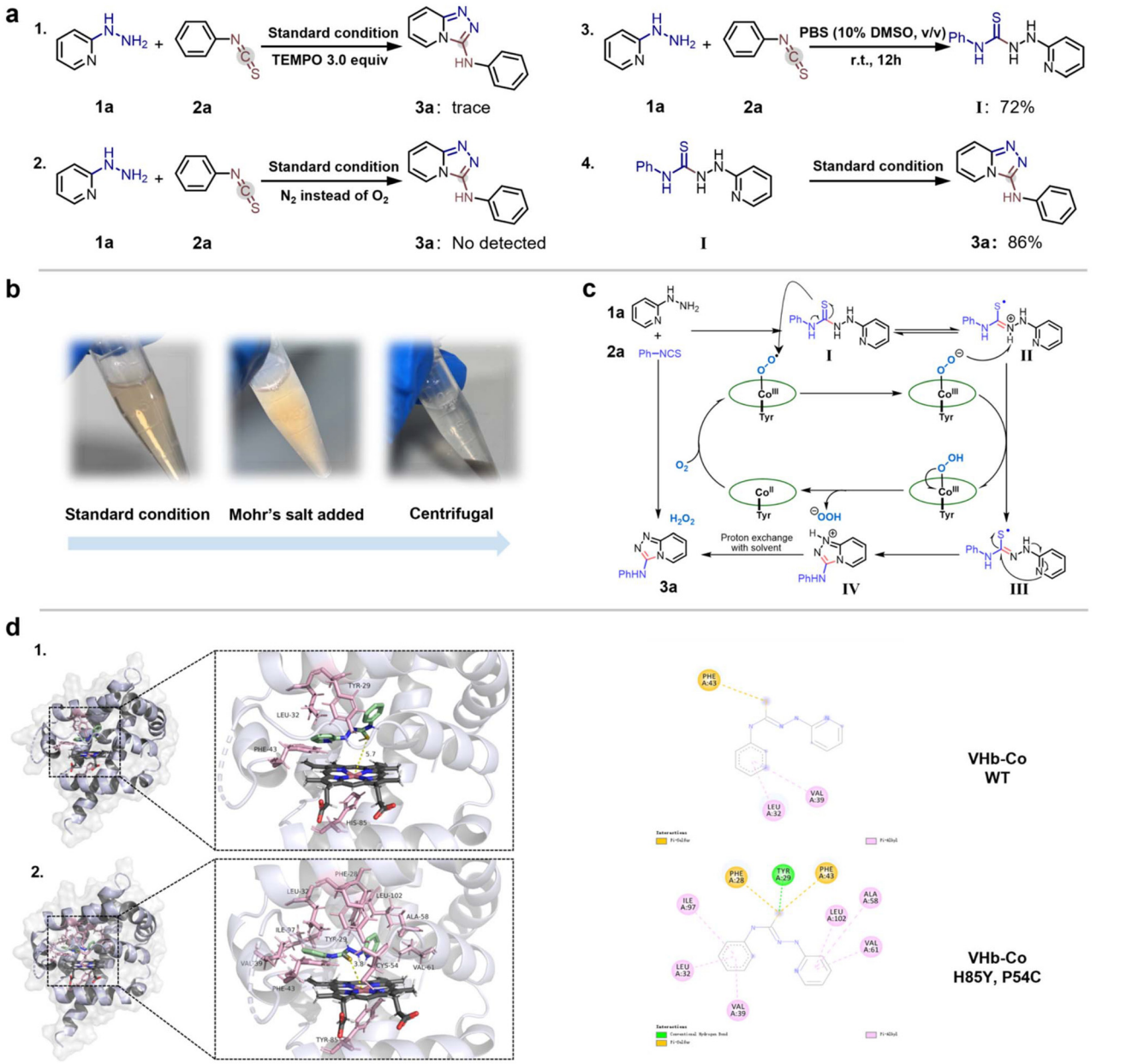

Fig. 3 (a) Control experiments. (b) Verification of hydrogen peroxide generation. (c) Proposed mechanism. (d). Structure model of thiourea intermediate **II** (light green) in the active site of VHb-Co. (1) Structure of WT-VHb-Co in complex with intermediate **II**. (2) Structure of VHb-Co (H85Y, P54C) in complex with intermediate **II**.

atom on intermediate **II** is at a relatively large distance from the metal center of Co(ppIX) (5.7 Å), and this steric hindrance significantly restricts the efficiency of the oxidation step. In contrast, as a key axial amino acid residue in the active cavity that is crucial for VHb-substrate binding and mediating the catalytic reaction, the H85Y mutation exerts a synergistic effect together with the P54C mutation, which plays an auxiliary optimization role, collectively inducing significant conformational rearrangement and optimization of the active cavity in VHb-Co (H85Y, P54C) and thereby forming a more compact and highly specific interaction network with intermediate **II**. Specifically, this structural adjustment stabilizes the conformation of the intermediate through hydrogen bonds, pi-sulfur interactions, and pi-alkyl interactions among the surrounding residues. Notably, the H85Y axial mutation precisely optimizes the spatial arrangement of the active cavity along the axial dimension, directly reducing the steric hindrance of intermediate **II** and effectively shortening the distance between intermediate **II** and the Co(ppIX) metal center. These conformational changes decrease the steric hindrance of intermediate **II**, bringing it closer to the metal center of Co(ppIX) (3.8 Å), which may further enhance catalytic efficiency (Fig. 3d-2).

Based on literature reports and the aforementioned experimental results, a plausible reaction mechanism for the VHb-Co (H85Y, P54C)-catalyzed synthesis of 3-amino-[1,2,4]-triazolo [4,3-*a*]pyridine compounds is proposed (Fig. 3c). Initially, 2-hydrazinopyridine (**1a**) undergoes a spontaneous nucleophilic addition reaction with phenyl isothiocyanate (**2a**), resulting in the formation of thiourea intermediate **I**. Under aerobic conditions, the Co(ppIX) cofactor interacts with O_2 to generate a Co^{3+}–superoxide intermediate, which subsequently acidifies intermediate **I**. The sulfur radical **II** is formed *via* an electron transfer process. Intermediate **II** is then converted to intermediate **III** through proton transfer, followed by intramolecular cyclization of intermediate **III** to form intermediate **IV**, accompanied by the generation of superoxide anions. Finally, intermediate **IV** undergoes proton exchange with the solvent, ultimately completing the cyclodesulfurization reaction to yield the target product **3a**.

Following the above screening and mechanistic clarification, the substrate scope of the reaction was explored using the VHb-Co (H85Y, P54C) mutant (Fig. 4). The applicability of substituents on the N-atom of isothiocyanates was first evaluated. Experiments showed that under standard reaction conditions, 2-hydrazinopyridine (**1a**) and phenyl isothiocyanate derivatives (**2**) could be efficiently converted to a series of 1,2,4-triazolopyridine derivatives (**3**) catalyzed by the biocatalyst. For monosubstituted phenyl isothiocyanates, *ortho*-, *meta*-, and *para*-substituents had minimal effect on the yield (**3b–3d**, 63%–72%). The influence of electron-donating (EDG) and electron-withdrawing (EWG) groups on the reaction yield was negligible (**3e–3g**), and even with a strong EWG like CF_3, the corresponding product yield still reached 68%. The yield decrease for **3h** and **3i** was likely attributed to the steric hindrance of 2,6-dimethyl and 2,4,6-trimethyl substituents, which hindered the substrate from binding to the active cavity of VHb and is consistent with the molecular docking results that steric hindrance restricts substrate-enzyme interaction efficiency. Additionally, the lower catalytic product yields with aliphatic isothiocyanates (**3j–3l**, 51%–62%) might be due to the poor reactivity of aliphatic substrates.

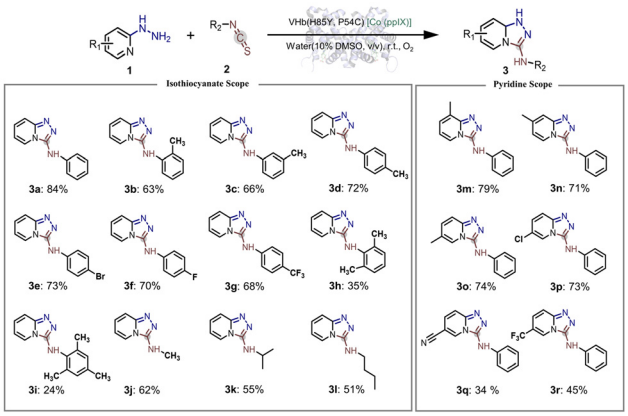

Fig. 4 Substrate scope. Reaction condition: 2-hydrazinopyridine (**1**, 0.05 mmol), isothiocyanate (**2**, 0.05 mmol), VHb-Co (H85Y, P54C) (Co(ppIX) containing 0.05 mol%), PBS (50 mM, 10% DMSO v/v), rt, O_2, 12 h.

Furthermore, other 2-hydrazinopyridine substrates were evaluated in this study. The results indicated that the nature of substituents on the pyridine ring exerted a significant effect on the reaction efficiency, 2-hydrazinopyridines bearing electron-donating groups or halogen substituents afforded good catalytic product yields (**3m–3p**, 71%–79%). In contrast, substrates with strong electron-withdrawing groups (such as –CN and $-CF_3$) showed a marked decrease in product yields. This discrepancy was attributed to the electron-withdrawing groups significantly reducing the electron density of the pyridine ring, thereby decreasing substrate reactivity and inhibiting the cyclodesulfurization reaction (**3q–3r**, 34%–45%).

These results are consistent with the proposed mechanism, in which electron transfer and the formation of intermediates are highly dependent on the electron density of the substrate. Furthermore, we systematically evaluated the industrial application potential of the cyclodesulfurization reaction catalyzed by VHb-Co (H85Y, P54C), and this study investigated the applicability of the VHb-catalyzed reaction at the gram-scale. Specifically, a gram-scale experiment was performed using 5.0 mmol of **1a** and **2a**, with both the catalyst and solvent scaled up proportionally from the small-scale reaction. The mixture was stirred at 800 rpm in a 500 mL glass vessel. The target product **3a** was successfully synthesized with a yield of 79%.

Conclusions

In summary, this study developed a green approach for synthesizing 3-amino-[1,2,4]-triazolo[4,3-*a*]pyridine through cyclodesulfurization catalyzed by engineered VHb in aqueous media under an oxygen atmosphere, facilitated by systematic screening of an artificial mutant enzyme library. This strategy effectively avoids the use of toxic reagents, metal catalysts, and harsh reaction conditions and achieves a low *E*-factor, adhering strictly to the principles of green chemistry. Compared to wild-type VHb, the selected VHb variant reconstituted with Co(ppIX) (VHb-Co (H85Y, P54C)) exhibits superior stability, catalytic activity, and a broad substrate scope. The molecular docking results of VHb-Co with intermediate **II** further provide theoretical support for the mechanism underlying its enhanced reaction activity. This method not only offers an innovative strategy for the green synthesis of nitrogen-containing heterocycles but also significantly expands the scope of non-natural reactions catalyzed by artificial metalloenzymes through the synergistic mechanism of precise regulation of the protein cavity and the expansion of the functions of artificial cofactors. Future studies may further optimize enzymatic efficiency *via* directed evolution to promote the in-depth application and industrialization of biocatalysis in organic synthesis.

Author contributions

Xinjia Yu: writing, methodology, docking simulation and investigation; Yutong Li: writing, methodology and investi-

gation; Shenhan Xie: investigation; Fengxi Li & Lei Wang: conceptualization, supervision, project administration, resources, and writing – review & editing.

Conflicts of interest

There are no conflicts to declare.

Data availability

The data supporting this article have been included as part of the supplementary information (SI). Supplementary information is available. See DOI: https://doi.org/10.1039/d5gc06364g.

Acknowledgements

This research was supported by: Technology Cooperation High-Tech Industrialization Project of Jilin Province and the Chinese Academy of Sciences (2025SYHZ0031).

References

1 (*a*) J.-Y. Liu, H.-E. Zhang, C. Wang, P.-F. Zhang, Y.-G. Xu, L. Shi and L.-P. Sun, *Eur. J. Med. Chem.*, 2025, **285**, 117272; (*b*) G. Frey, S. Rits-Volloch, X.-Q. Zhang, R. T. Schooley, B. Chen and S. C. Harrison, *Proc. Natl. Acad. Sci. U. S. A.*, 2006, **103**, 13938–13943.

2 (*a*) Y. Hu, L. Chen, C. Zou, J. He, L. Feng, J.-Q. Wu, W.-H. Chen and J. Hu, *Org. Lett.*, 2022, **24**, 5137–5142; (*b*) Y. Zhang, X. Luo, M. Zhu, Z. Zhu, Y. Zou, X. Liu and J. Chen, *J. Agric. Food Chem.*, 2025, **73**, 1813–1823; (*c*) N. R. Bandaru, P. Makam, P. Akshinthala, N. K. Katari, V. Banoth, B. Kolli and R. Gundla, *Molecules*, 2022, **27**, 7647; (*d*) C. Tian, G. Zhang, Z. Xia, N. Chen, S. Yang and L. Li, *Eur. J. Med. Chem.*, 2022, **231**, 114122.

3 (*a*) E. Li, Z. Hu, L. Song, W. Yu and J. Chang, *Chem. – Eur. J.*, 2016, **22**, 11022–11027; (*b*) S. Jiao, Z. Wang, Q. Zhao, W. Yu and J. Chang, *Tetrahedron*, 2018, **74**, 3069–3073; (*c*) Y. Xu, B. Shen, L. Liu and C. Qiao, *Tetrahedron Lett.*, 2020, **61**, 151844.

4 X. Yu, S. Xie, C. Wang, Z. Wang, F. Li and L. Wang, *Org. Lett.*, 2025, **27**, 9335–9340.

5 M. Tobiszewski, W. Przychodzeń, M. Bystrzanowska and M. J. Milewska, *Green Chem.*, 2021, **23**, 9583–9588.

6 (*a*) L. Tang, X. Yang, N. Sun, G. Wu, Y. Wu and F. Zhong, *Chin. J. Chem.*, 2024, **42**, 2335–2340; (*b*) Y. Fu, X. Liu, Y. Xia, X. Guo, J. Guo, J. Zhang, W. Zhao, Y. Wu, J. Wang and F. Zhong, *Chem*, 2023, **9**, 1897–1909; (*c*) X. Yang, J. Huang, J. Guo, S. Fang, Z. Wang, G. Wu, Y. Wu and F. Zhong, *Chem. Soc. Rev.*, 2025, **54**, 5157–5188; (*d*) F. Li, Y. Dai, S. Xie, X. Yu, X. Shi, Z. Li, C. Du, Z. Wang and L. Wang, *Green Chem.*, 2025, **27**, 7229–7233; (*e*) B. Chen, Q. Zhang, J. Yu, B. Zhao, R. Ge, Z. Zhang, D. Luo, B. Wang and X. Huang, *Nat. Catal.*, 2025, **8**, 740–748; (*f*) Y. Tang, Y. Zeng, C. Wang, Z. Wang, D. Zhao, C. Du, F. Li and L. Wang, *ACS Catal.*, 2025, **15**, 17726–17737; (*g*) Y. Xu, F. Liu, B. Zhao and X. Huang, *Chin. J. Chem.*, 2024, **42**, 3553–3558; (*h*) Y. Zhou, Y. Li, J. Wen, Y. Zhang, Z. Hu, K. Zhong, H. Cao and J. Cheng, *Chin. J. Chem.*, 2025, **43**, 1479–1486.

7 (*a*) H. R. Valentino, L. Qian, J. M. Parks, E. E. Drufva, A. Sedova, P. S. Mehta, M. P. Watson, R. J. Giannone, S. S. Galanie and J. K. Michener, *Green Chem.*, 2025, **27**, 6283–6292; (*b*) A. Schiefer, L. Schober, T. Rohr, M. Winkler and F. Rudroff, *Green Chem.*, 2025, **27**, 10234–10241; (*c*) F. Della-Felice and G. Roelfes, *Nat. Catal.*, 2025, **8**, 633–634; (*d*) D. Deng, Z. Jiang, L. Kang, L. Liao, X. Zhang, Y. Qiao, Y. Zhou, L. Yang, B. Wang and A. Li, *Nat. Catal.*, 2025, **8**, 20–32; (*e*) Z. Zhang, Q. Zhang, T. Wang, B. Zhao, B. Chen, X. Wang, J. Chun, T. Zhang, B. Wang and X. Huang, *ACS Catal.*, 2025, **15**, 12684–12690; (*f*) B. Chen, R. Li, J. Feng, B. Zhao, J. Zhang, J. Yu, Y. Xu, Z. Xing, Y. Zhao, B. Wang and X. Huang, *J. Am. Chem. Soc.*, 2024, **146**, 14278–14286; (*g*) B. Rassati, J. Reusser, L. Robustini, O. Ben Mariem, A. Pavlova, I. Eberini and F. Paradisi, *ACS Catal.*, 2025, 21115–21123, DOI: 10.1021/acscatal.5c07706; (*h*) Y. Tang, Y. Xu, X. Zhang, C. Wang, D. Zhao, F. Li and L. Wang, *ACS Catal.*, 2025, **15**, 4784–4797; (*i*) Y. Dai, C. Zhang, X. Yu, C. Du, F. Li and L. Wang, *Green Chem.*, 2025, **27**, 15582–15587; (*j*) J. Peng, T. Hao, W. Ma, Z. Xu and T. Li, *Chin. J. Chem.*, 2025, **43**, 33–38.

8 (*a*) H. Keum, J. Kim, Y. H. Joo, G. Kang and N. Chung, *Chemosphere*, 2021, **268**, 128795; (*b*) T. Tang, H. Fan, S. Ai, R. Han and Y. Qiu, *Chemosphere*, 2011, **83**, 255–264; (*c*) F. Li, Y. Xu, Y. Xu, H. Xie, J. Wu, C. Wang, Z. Li, Z. Wang and L. Wang, *Org. Lett.*, 2023, **25**, 7115–7119; (*d*) S. Fan, M. Qin, Q. Wang, Y. Jiang and Z. Cong, *ACS Catal.*, 2025, **15**, 2977–2986; (*e*) R. Singh, J. N. Kolev, P. A. Sutera and R. Fasan, *ACS Catal.*, 2015, **5**, 1685–1691; (*f*) A. Tinoco, V. Steck, V. Tyagi and R. Fasan, *J. Am. Chem. Soc.*, 2017, **139**, 5293–5296; (*g*) A. Tinoco, Y. Wei, J.-P. Bacik, D. M. Carminati, E. J. Moore, N. Ando, Y. Zhang and R. Fasan, *ACS Catal.*, 2019, **9**, 1514–1524; (*h*) E. J. Moore, V. Steck, P. Bajaj and R. Fasan, *J. Org. Chem.*, 2018, **83**, 7480–7490.

9 (*a*) Q. Chen, J. Yu, S. Li, C. Wang, P. Zheng and H.-J. Pan, *ChemCatChem*, 2025, **17**, e00901; (*b*) P. Du, J. Li, T.-P. Zhou, J. Wang, W. Hu, H. Li, B. Wang and H.-J. Pan, *Nat. Catal.*, 2025, **8**, 822–832.

10 (*a*) M. Bordeaux, R. Singh and R. Fasan, *Bioorg. Med. Chem.*, 2014, **22**, 5697–5704; (*b*) G. Sreenilayam, E. J. Moore, V. Steck and R. Fasan, *ACS Catal.*, 2017, **7**, 7629–7633.

11 (*a*) H. Xie, K. Liu, Z. Li, Z. Wang, C. Wang, F. Li, W. Han and L. Wang, *JACS Au*, 2024, **4**, 4957–4967; (*b*) Y. Xu, F. Li, H. Xie, Y. Liu, W. Han, J. Wu, L. Cheng, C. Wang, Z. Li and L. Wang, *Chem. Sci.*, 2024, **15**, 7742–7748; (*c*) H. Xie, F. Li, Y. Xu, C. Wang, Y. Xu, J. Wu, Z. Li, Z. Wang and L. Wang,

Green Chem., 2023, **25**, 6853–6858; (*d*) F. Li, Q. Sun, Z. Yu, S. Xie, W. Kan, Z. Li, C. Du, Z. Wang and L. Wang, *Chin. J. Chem.*, 2025, **43**, 2143–2150.

12 (*a*) Y. Xu, F. Li, N. Zhao, J. Su, C. Wang, C. Wang, Z. Li and L. Wang, *Green Chem.*, 2021, **23**, 8047–8052; (*b*) Y. Xu, F. Li, H. Xie, Y. Liu, W. Han, J. Wu, L. Cheng, C. Wang, Z. Li and L. Wang, *Chem. Sci.*, 2024, **15**, 7742–7748.

13 A. Tinoco, Y. Wei, J.-P. Bacik, D. M. Carminati, E. J. Moore, N. Ando, Y. Zhang and R. Fasan, *ACS Catal.*, 2019, **9**, 1514–1524.

14 U. Chacon-Argaez, M. A. Alvarez-Amparán and L. Cedeño-Caero, *Chemosphere*, 2024, **362**, 142791.

15 (*a*) O. Trott and A. J. Olson, *J. Comput. Chem.*, 2010, **31**, 455–461; (*b*) E. F. Pettersen, T. D. Goddard, C. C. Huang, G. S. Couch, D. M. Greenblatt, E. C. Meng and T. E. Ferrin, *J. Comput. Chem.*, 2004, **25**, 1605–1612; (*c*) A. Waterhouse, M. Bertoni, S. Bienert, G. Studer, G. Tauriello, R. Gumienny, F. T. Heer, T. A P. de Beer, C. Rempfer, L. Bordoli, R. Lepore and T. Schwede, *Nucleic Acids Res.*, 2018, **46**, W296–W303.